Electronic Supplementary Information (ESI) for

Technoeconomic Analysis of Metal–Organic Frameworks for Bulk Hydrogen Transportation

Aikaterini Anastasopoulou,[a] Hiroyasu Furukawa,[b,c] Brandon Barnett,[b,c] Henry Jiang,[b,c] Jeffrey R. Long[b,c] and Hanna M. Breunig[*a]

[a]*Energy Analysis and Environmental Impacts Division, Lawrence Berkeley National Laboratory, Berkeley, CA 94720, USA. E-mail: hannabreunig@lbl.gov*
[b]*Department of Chemistry, University of California, Berkeley, CA 94720, USA*
[c]*Materials Sciences Division, Lawrence Berkeley National Laboratory, Berkeley, CA 94720, USA*

Table of Contents

26 pp.
11 tables
8 figures

1. Methodology & Approach

This study conducts a technoeconomic analysis of the storage and transportation of hydrogen (H_2) by means of high pressure compressed H_2 (Comp-H_2) gas trucks, cryogenic liquid H_2 (Liq-H_2) trucks, and adsorption-based trucks transporting H_2 using metal–organic framework (MOF-H_2) packed tube trailers at low temperatures and high pressures (MOF–H_2). For the MOF truck systems, we use Ni_2(*m*-dobdc)[1] and MOF-5[2] as representative materials. We excluded results for Ni_2(dobdc), Co_2(dobdc) and Co_2(*m*-dobdc), which were also assessed, as the results were well represented by Ni_2(*m*-dobdc). A delivery rate of 50,000 kg H_2/day is modeled in the base case. The cost of H_2 delivery is estimated for two delivery supply chains: long-distance transmission and "last-mile" distribution. A supply chain coupling transmission and distribution is provided in the sensitivity analysis (Section 3.2). The system boundaries of these delivery supply chains, which are presented in Fig. 1 (main text), start at the gas terminal where H_2 is loaded onto trucks, and ends at either the unloading at an industrial end-use or the unloading and storage at distributed refueling stations. A detailed description of the methodology and assumptions used to model and couple each system component is provided in the sections below.

1.1 Hydrogen Delivery Supply Chains

The system boundary for the long-distance transmission supply chain begins at the gas terminal near the point of H_2 production. The gas terminal includes equipment for the storage and compression and cooling (for MOF–H_2 and Comp-H_2 trucks) or liquefaction (Liq-H_2 trucks) of pure hydrogen. Hydrogen is assumed to be delivered to the gas terminal at a pressure of 20 bar and 294 K, reflecting supply from a large scale fossil or renewably fueled H_2 production facility[3] with geological cavern storage. The capital and operating costs associated with H_2 production, geological storage and the end-use application are not included in the transmission delivery cost. Compressors and cooling equipment used for charging the trucks are also used to fill the above ground storage tanks (Table S1).

The system boundary for the last-mile distribution supply chain includes a city-gate terminal through to the refueling stations. The city-gate terminal is modeled in the same way as the gas terminal for the transmission supply chain, described above, with the main difference being the H_2 feed conditions. In this case, we assume a pipeline delivers H_2 from a H_2 production facility or large storage cavern to the city-gate terminal at a pressure of 48 bar and temperature of 298 K, as considered in the Argonne National Laboratory (ANL) Hydrogen Delivery Station Analysis Model (HDSAM).[4] The capacity (dispensing rate) of refueling stations is determined based on the amount of H_2 that can be supplied in a single delivery each day by each examined delivery technologies. More precisely, the MOF–H_2 trucks at 200 K serve refueling stations of 100 kg H_2/day, while the Comp-H_2-500 bar and Liq-H_2 trucks serve refueling stations of 1,300 and 3,000 kg H_2/day, respectively. The Comp-H_2-350 bar trucks serve refueling stations of 600 kg H_2/day. Finally, the Ni_2(*m*-dobdc)-H_2 and MOF-5 trucks at 77 K serve refueling stations of 200 kg H_2/day and 300 kg H_2/day, respectively. In the case of MOF-based H_2 and Comp-H_2 delivery, it is assumed that a full tube trailer will be exchanged with a waiting, empty trailer at the refueling station, which is operated at 350 bar. The H_2 tube trailers delivered by the Comp-H_2 trucks are assumed to serve as primary storage units at the same operating pressure (350 bar) or higher (500 bar) and ambient temperature.[5–7] On the other hand the desorbed H_2 gas from the MOF-H_2 tube trailers is re-pressurized at the refueling station for transfer to storage vessels at 350 bar and 25 °C. In the case of the "high packing density" scenario (discussed further in Section 2.1 below), the gas can be desorbed at a relatively higher pressure (>20 bar). In that case, we assume the gas is stored at the compressor discharge temperature, which is less than

25°C. Equipment costs associated with gas re-pressurization and additional storage are not explicitly modeled in this analysis, as we assume the equipment already captured in the refueling station Hydrogen Refueling Station Analysis Model (HRSAM) from ANL can be used for this process.[8]

In the context of this study, the HRSAM is used to estimate capital and operating costs of refueling stations at the selected capacities.[8] These capacities fall within range of refueling stations studied in previous analysis.

Finally, in the sensitivity analysis we model a supply chain where trucks deliver H_2 from a gas terminal near a source of H_2 to refueling stations (transmission-distribution). Distances used in the transmission and distribution supply chains are assumed, however constraints on truck and driver availability greatly affects the number and ratio of truck trailers and driver cabins (cabs) required. Details on this supply chain discussed in the following sections.

Table S1 Assumptions for studied H_2 delivery technologies.

Model Parameter	Value	Reference
	MOF–H_2 System	
Storage pressure	160 bar	DOE technical target[9]
Truck pressure	100 bar	
Truck temperature	200 K, 77 K	
Tube cost	$7,682*	Tankinator[10,a]
H_2 storage - amount	50% of daily delivery rate	[11]
Storage tank cost	$944/kg H_2*	DOE technical target [9]
Pick-up/drop-off time	1.5 h/trip	HDSAM[4]
	Comp-H_2 System	
Storage pressure	430 bar	DOE technical target[9]
Truck pressure	350 bar, 500 bar	
Truck temperature	298 K	
Tube cost	$26,126 (350 bar), $38,283 (500 bar)*	Tankinator[10,a]
H_2 storage - amount	50% of daily delivery rate (kg H_2)	[11]
Storage tank cost	$1,221/kg H_2*	DOE technical target[9]
Pick-up/drop-off time	1.5 h/trip	HDSAM[4]
	Liq-H_2 System	
Truck pressure & temperature	Atmospheric pressure & cryogenic temperature	
Tank cost (incl. trailer)	$211/kg H_2*	DOE technical target[9]
H_2 storage amount	200% of daily delivery rate (kg H_2)	[11]
Storage tank cost	$51/kg H_2*	[11]
Load time	3 h/trip	HDSAM[4]
Unloading time	3.5 h/trip	HDSAM[4]

* 2020 dollar value.

[a] tube cost estimated for a 12.19 m tube length and 0.56 m tube diameter

1.2. Adsorption (MOF–H_2) System Model

We model the MOF–H_2 system as a 9-tube trailer truck, which is commonly employed for gaseous H_2 transport.[12] The tubes are assumed to be packed with the MOF material, where H_2 can be adsorbed and stored under specific operating conditions. The design of the MOF–H_2 systems considers a maximum truck gross weight limit of 80,000 pounds (36,287 kg), as imposed by federal regulations.[13] In the absence of adsorption column data for benchmarking, we estimate the amount of adsorbent material and adsorbed H_2 per truck mathematically in MATLAB software.[14] The tubes are modeled as packed beds according to the design specifications presented in Table 1 (main text). The H_2 adsorption system is evaluated for five MOFs—Ni_2(*m*-dobdc), Ni_2(dobdc), Co_2(dobdc), Co_2(*m*-dobdc), and MOF-5—at a pressure of 100 bar and a temperature of 200 K and 77 K. Results for Ni_2(dobdc), Co_2(dobdc), Co_2(*m*-dobdc) are excluded from the figures as they are very similar to Ni_2(*m*-dobdc).

The Hydrogen Storage Engineering Center of Excellence (HSECoE) has developed tools for modelling the H_2 adsorption system for onboard passenger vehicle systems.[10] More precisely, the "adsorbent storage system design–standalone" model enables the evaluation of the adsorption tank system, as a packed or fluidized bed, under different operating conditions. Additionally, the "tankinator" excel tool[10] estimates the geometry and mass of the storage tank based on the desired tank height and radius, and the maximum tank temperature. The aforementioned tools consider MOF-5 as the adsorbent material and use the modified Dubinin-Astakhov equation[15,16] or fitting adsorption data. Our model builds on this work and provides the ability to estimate adsorption and desorption times for a given adsorbent, operating conditions, and bed geometry. Additionally, developing a model that could integrate different isotherm models required us to build our own system of equations in MATLAB software,[14] described in more detail below. In our novel adsorption model, we combine key assumptions derived from similar studies of adsorption systems as well as recent experimental data.[1,2] The following key assumptions are made:[17–20]

- System performs under isothermal conditions
- Particles are characterized by density and size homogeneity
- Velocity and concentration profiles are uniform in the bed
- Flow pattern follows the axial dispersion model
- The physical properties of the fluid are constant

The concentration of H_2 in the bulk fluid phase of the packed bed is estimated from the dimensionless material balance equation (Eq. S1).[21]

$$\frac{\partial C_g}{\partial \tau} = \frac{1}{\mathrm{Pe}} \frac{\partial^2 C_g}{\partial z^2} - \frac{\partial C_g}{\partial z} - \mu \frac{\partial N}{\partial t} \qquad \text{(S1)}$$

Here, $\tau = u \cdot t \cdot L^{-1}$ is dimensionless time (t = time, L = bed length, and u = superficial gas velocity)

z = dimensionless distance, $z = x/L$ (x = distance from bed inlet)

$C_g = c_g/c_0$ is dimensionless adsorbate concentration in the bulk gas phase (c_g = adsorbate concentration in bulk gas phase, c_0 = initial adsorbate concentration in the bed inlet)

Pe is the Peclet number which is estimated by empirical correlations provided in Table S7

$\mu = [(1 - \varepsilon_b)\cdot \varepsilon_b^{-1}\cdot\rho_p]\cdot n_0\cdot c_0^{-1}$ (ε_b = bed porosity, ρ_p = particle density, n_0 = initial adsorbate concertation in the solid phase);

and $N = n/n_0$ is the dimensionless adsorbate concentration in solid phase (n = adsorbate concentration the in solid phase).

The boundary and initial conditions of Eq. S1 for the adsorption process are provided below.[21]

Adsorption:

$$at\ \tau = 0,\ C_g = C1 \text{ for all } z$$

$$at\ z = 0,\ C_g = 1 \text{ for all } t$$

$$at\ z = 1,\ \frac{\partial C_g}{\partial z} = 0 \text{ for all } t$$

Desorption by depressurization:

$$at\ \tau = 0,\ C_g = 1 \text{ for all } z$$

$$at\ z = 0,\ C_g = C_{des} \text{ for all } t$$

$$at\ z = 1,\ \frac{\partial C_g}{\partial z} = 0 \text{ for all } t$$

Here, $C1$ is the dimensionless gas concentration remaining in the packed bed upon desorption and C_{des} is the dimensionless gas concentration estimated based on the selected desorption pressure.

The operation of the adsorption system is established for a bed saturation level of 95% ($C_g = c_g/c_0 = 0.95$), which is a common consideration for adsorption beds.[22–26] The total amount adsorbed ($m_{adsorbed}$) in the bed is calculated from Eq. S2:

$$m_{adsorbed} = Q \cdot c_0 \int_0^{t_1} \left(1 - \frac{c_g}{c_0}\right) dt \qquad (S2)$$

where Q is the gas flow rate and t_1 denotes the time where c_g/c_0 is equal to 0.95, estimated from the breakthrough curve as generated by Eq. S1.

The mass of adsorbent ($m_{adsorbent}$) is estimated based on the following equation:

$$m_{adsorbent} = V_{bed} \cdot \rho_{bulk} \qquad (S3)$$

Here, V_{bed} denotes the volume of the bed, which is estimated based on the bed length and diameter, and ρ_{bulk} is the bulk density (packing density) of the packed bed (structured packing), which is estimated by:

$$\rho_{bulk} = (1 - \varepsilon_b) \cdot \rho_p \qquad (S4)$$

where:

$$\rho_p = \left(1 - \varepsilon_p\right) \cdot \rho_s \qquad \text{(S5)},$$

ε_p is the internal porosity, and ρ_s is the single crystal density. The base case study considers a bed porosity of ε_b = 0.6 and pellet porosity ε_p = 0.2. The single crystal density of MOF-5 is 0.605 g/cm^3, and for Ni_2(*m*-dobdc) ρ_s = 1.19 g/cm^3.[27,28] These values give base bulk densities of 0.19 and 0.38 g/cm^3 for MOF-5 and Ni_2(*m*-dobdc), respectively.

In adsorption systems, the gas−solid equilibrium is typically described by the experimentally-determined isotherm data. In the given case study, the amount of H_2 adsorbed in MOF-5 and Ni_2(*m*-dobdc) as a function of pressure was modeled using a dual-site Langmuir fit, represented by Eq. S6.

$$n = \frac{A_1 \cdot B_1 \cdot (c_0 \cdot C_g \cdot k)^{n_1}}{1 + B_1 \cdot (c_0 \cdot C_g \cdot k)^{n_1}} + \frac{A_2 \cdot B_2 \cdot (c_0 \cdot C_g \cdot k)^{n_2}}{1 + B_2 \cdot (c_0 \cdot C_g \cdot k)^{n_2}} \qquad \text{(S6)}$$

The resulting fit parameters are provided in Table S2 for MOF-5 and Ni_2(*m*-dobdc) under select operating conditions. Experimental isotherm data and dual-site Langmuir fits are presented in Figs. S1–S3.

Assuming the presence of a local equilibrium between the mobile and adsorbed phases of H_2, the adsorption rate, $\frac{\partial N}{\partial t}$, can be given by Eq. S7.[29]

$$\frac{\partial N}{\partial \tau} = \frac{\partial N}{\partial C_g} \cdot \frac{\partial C_g}{\partial \tau} \qquad \text{(S7)}$$

Eq. S6 and Eq. S7 can then be incorporated in the mass balance equation (Eq. S1), and the resulting partial differential equation can be solved in MATLAB software, employing the in-built function “pdepe.”

Table S2 Parameters determined from the dual-site Langmuir isotherm model.

MOF	k^a (m^3·bar/mol)	A_1 (mol/kg)	B_1 (bar^{-n1})	n_1	A_2 (mol/kg)	B_2 (bar^{-n2})	n_2	Q_{st} (kJ/mol)	SSE^b
Ni_2(*m*-dobdc) (200)*	0.0167	6.98	0.0673	1	3.73	0.0126	0.570	–12.3[27]	0.562
MOF-5 (200 K)	0.0165	24.5	0.0052	1	24.5	0.0029	1	–4[28]	0.009
Ni_2(*m*-dobdc) (77 K)	0.0063	22.7	0.0402	0.457	19.4	0.974	0.575	–12.3[27]	0.078
MOF-5 (77 K)	0.0064	29.0	0.187	0.943	28.7	0.0717	0.998	–4[28]	8.711

[a] $k = RT \times 10^{-5}$ (assuming ideal gas behavior); [b] SSE = sum of squared error

*Isotherm parameters B1 and B2 are estimated by fitting all temperature isotherm data within range of 200K and 373 K based on the following equations: B_1=k1·exp(E1/(R·T)) and B_2= k2·exp(E2/(R·T)) , where k1=4.011E-05 bar^{-n1}, E1=1.237e+04 J/mol, k2= 0.001 bar^{-n2}, E2=4.125e+03 J/mol, R=8.314 J/(mol·K) and 200K ≤ T≤ 373K

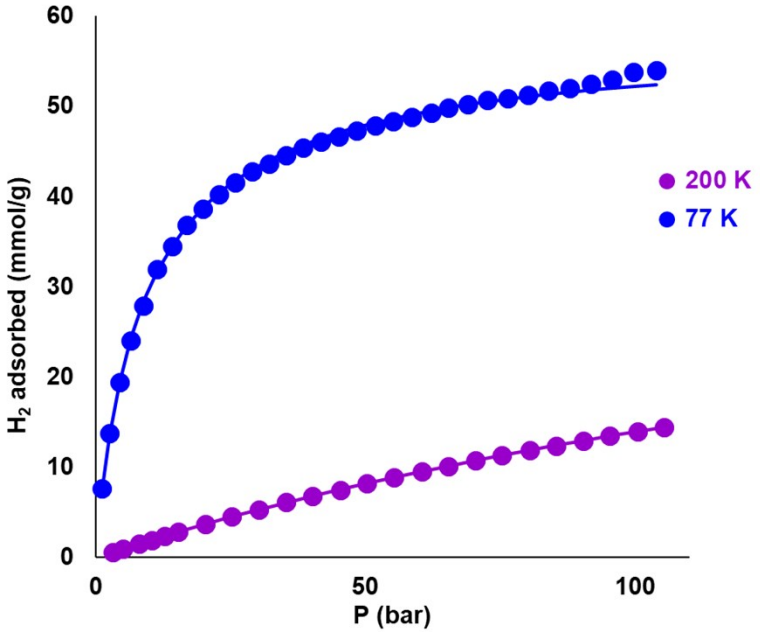

Fig. S1 Experimental adsorption isotherms for H_2 uptake in MOF-5 at 77 and 200 K (solid markers). Solid lines represent fits with a dual-site Langmuir model (see Table S2). P: pressure.

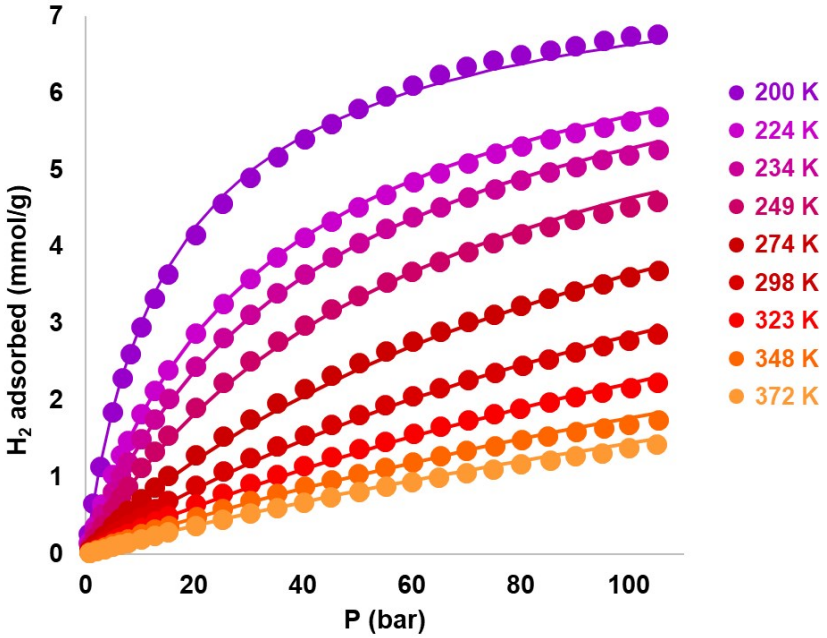

Fig. S2 Experimental adsorption isotherms for H_2 uptake in Ni_2(*m*-dobdc) at 200, 224, 234, 249, 274, 298, 323, 348 and 372 K (solid markers). Solid lines represent dual-site Langmuir fits (see Table S2). P: pressure.

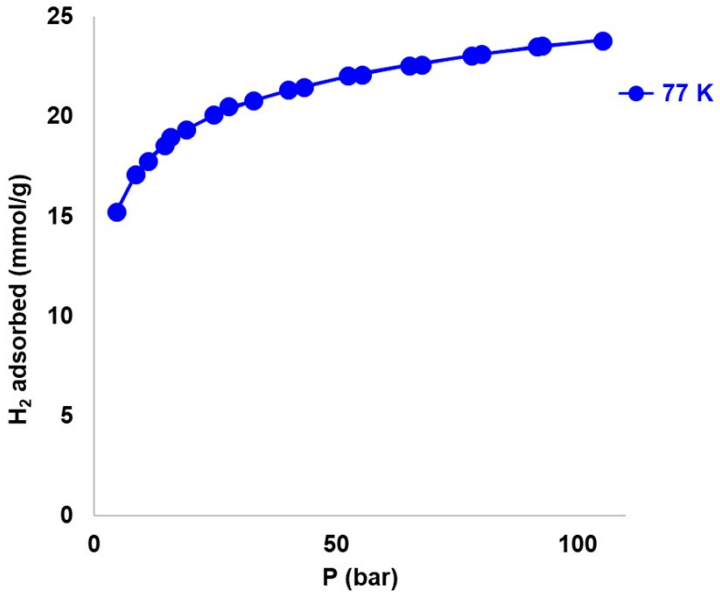

Fig. S3 Experimental adsorption isotherms of Ni_2(*m*-dobdc) at 77 K (solid markers). The solid line represents the dual-site Langmuir fit (see Table S2) P: pressure.

1.3 Trucking Delivery Logistics

For each supply chain, delivery technology, and market size, it is necessary to estimate the total number of truck cabs, trailers, and refueling stations (Table S3). This capital cost is largely driven by the capacity of each system to deliver H_2 in a single trip, and the number of hours required to make a round trip. Drivers and trucks are assumed to have a limited availability per day based on regulations set for consecutive driving hours and breaks, and maintenance. For the transmission supply chain, we consider distances between 25 and 300 km (base of 100 km), and 1 and 50 km (base of 1 km) for the distribution supply chain. We assume driving speeds of 85 and 50 km/h for the transmission and distribution delivery mode, respectively.

The number of truck cabs can be estimated based on the desired delivery capacity, the total round-trip duration, and a 14-hour daily truck availability. However, the number of trailers is a more nuanced parameter, and depends on whether the driver must wait with a trailer during discharge, or can switch trailers with a waiting empty trailer. When we developed the model, we explored both possibilities and quickly determined that trailer switching is critical for lowering costs. For long distance transmission, the number of trailers is simply double the number of cabs for the MOF–H_2 and Comp-H_2 systems.[11] In the distribution case, the respective number of trailers is equal to the number of truck cabs plus the number of refueling stations, as trucks are assumed to exchange a full tube trailer for an empty one at a refueling station.[7,11] For the Liq-H_2 system, the number of trailers is equal to the number of truck cabs as the driver does not leave the trailer for use as storage at the end point or refueling stations.[11]

Table S3 Number of trucks and refueling stations required for all considered H_2 systems (base case) for 50,000 kg H_2/day.

Component	Comp-H_2 350 bar	Comp-H_2 500 bar	Liq-H_2	Ni_2(*m*-dobdc) (200 K)	MOF-5 (200 K)	Ni_2(*m*-dobdc) (77 K)	MOF-5 (77 K)
Transmission							
Trucks (25 km)	29	23	13	776	1,034	133	82
Trucks (100 km, base case)	43	34	13	1164	1,551	170	122
Trucks (300 km)	86	67	13	2327	3,102	339	244
Distribution							
Trucks (1 km, base case)	27	20	11	585	780	86	62
Trucks (20 km)	35	27	21	780	1040	114	82
Trucks (50 km)	53	40	21	1170	1559	171	123
Refueling station capacity (kg H_2/day)	600	800	3000	100	100	200	300
Refueling stations	105	79	21	2,339	3,118	341	246

1.4 Capital and Operation Cost Estimates

1.4.1 Operation Costs

The total amount of gas requiring compression and cooling is determined based on the size of the market and required H_2 demand, and the assumed H_2 losses that occur along the supply chain. Energy costs associated with supply chains stem from the compression and cooling of the H_2 gas, the precooling of MOF-packed tube trailers, and any subsequent compression and cooling required at the refueling stations. The total amount of H_2 transported per truck is estimated by multiplying the number of tubes by the adsorbed H_2 mass per tube, as estimated by Eq. S2. Due to the exothermic character of the adsorption process, tube precooling and heat removal is required so as to enhance H_2 uptake during truck charging. We estimate the total cooling requirements per fleet include:

1) the total amount of heat that must be removed during the adsorption process. We estimate this as the H_2 adsorbed per truck per day, multiplied by the heat of adsorption, Q_{st}, of each MOF (Table S2). Any heat losses through the tube walls have been excluded from the study.

2) the precooling of the adsorbent packed beds. We estimate precooling requirements for each trailer employed per fleet, assuming an early morning, one-time precooling of each tube trailer from a temperature $T1$ to the desired adsorption temperature $T2$ (200 or 77 K); see Eq. S8 and S9. The initial temperature $T1$ is assumed to be 250 or 127 K in our base case for the 200 or 77 K operation temperatures,

respectively. The heat capacity of MOF-5 is given by Eq. S9 (units of kJ/(kg*K)), as reproduced from Ref. 30. The same heat capacity value was used to model the Ni_2(*m*-dobdc) system, due to limited data. While the cost of energy consumed to precool tube trailers is determined and included in operating expenses, the time required to precool the MOF material was not estimated in this analysis as we assume it is performed once overnight.

$$Q_{\text{bed}} = m_{\text{adsorbent}} \cdot \int_{T1}^{T2} \text{Cp}(T)\text{d}T \qquad \text{(S8)}$$

$$C_{\text{p,MOF-5}} = 0.524 - 8.885 \times 10^{-3} \cdot T + 9.624 \times 10^{-5} \cdot T^2 - 3.469 \times 10^{-7} \cdot T^3 + 4.417 \times 10^{-10} \cdot \text{T}^4 \qquad \text{(S9)}$$

It has been demonstrated[30] that the specific heat of MOF-5 is smaller at lower temperatures; At 77 and 200 K, we found specific heat values of 15 and 28.8 kJ/kg, respectively for the MOF–H_2 systems operated at 77 and 200 K.

Considering that the MOF-based H_2 delivery technology is at an early development stage, we estimate the energy costs assuming a conventional refrigeration system with a Carnot efficiency (η_C) calculated from Eq. S10.[31] The actual design of the cooling system for the MOF-based H_2 trucks is excluded from this analysis in the absence of a comprehensive heat transfer study.

The actual power requirements of the refrigeration system are estimated by dividing the cooling energy requirements (as reported in Table S4 and S5) by the Coefficient of Performance (COP), which is defined in Eq. S11. Here, T_{out} is the highest discharge temperature; and T_{R} is the lowest temperature of the refrigerant. In this study, the highest temperature of the refrigeration system was selected as 318 K, while the lowest temperatures investigated were 195 and 72 K for the MOF–H_2 systems operating at 200 K and 77 K, respectively.

$$\eta_{\text{C}} = -3.533 \times 10^{-9} \cdot T_{\text{R}}^{\,3} - 9.9354 \times 10^{-6} \cdot T_{\text{R}}^{\,2} + 3.2995 \times 10^{-3} \cdot T_{\text{R}} \qquad \text{(S10)}$$

$$COP = \frac{T_{\text{R}}}{(T_{\text{out}} - T_{\text{R}})} \cdot \eta_{\text{C}} \qquad \text{(S11)}$$

Other non-cooling operating costs of the trucks include maintenance and fuel costs. These costs, along with unit capital costs of the equipment and their utilities are presented in Table S6. Labor costs are grouped with the truck transportation component of the supply chain. In order to express cost in the 2020-dollar value, we apply relevant inflation rates and cost plant indices, as presented in Table S6. In terms of the capital investment, a discounted cash flow was carried out, including depreciation costs based on a Modified Accelerated Cost Recovery System method.[4]

Table S4 Energy requirements (in GJ) of H_2 delivery modes for transmission from the gas terminal for 50,000 kg H_2 /day (excluding the energy costs of the Comp-H_2 and Liq-H_2 storage).

Comp-H_2 Gas Terminal – Transmission							
	Comp-H_2 350 bar	Comp-H_2 500 bar	Liq-H_2	Ni_2(*m*-dobdc) (200 K)	MOF-5 (200 K)	Ni_2(*m*-dobdc) (77 K)	MOF-5 (77 K)
Compression							
(1) Cooling Energy	350	417	NA	238	238	333	333
(2) Refrigeration–Power[a]				626	626	6,167	6,167
(3) Electricity	363	435	NA	172	172	172	172
Adsorption-Cooling							
(4) Cooling Energy	NA	NA	NA	307	100	307	100
(5) Refrigeration–Power[a]	NA	NA	NA	808	263	5,685	1,852
Tube Precooling							
(6) Cooling Energy	NA	NA	NA	360	335	38	14
(7) Refrigeration–Power[a]	NA	NA	NA	947	882	704	259
Liquefaction							
(8) Electricity	NA	NA	1,651	NA	NA	NA	NA
Total Energy Consumption	713 (1+2)	852 (1+2)	1,651 (8)	2,553 (2+3+5+7)	1,943 (2+3+5+7)	12,728 (2+3+5+7)	8,450 (2+3+5+7)
Share of energy costs at gas terminal in total delivered H_2 energy content[b]	12%	14%	28%	43%	32%	212%	140%

[a]Refrigeration power requirements for the MOF–H_2 systems is estimated based on the cooling energy consumption divided by the COP value (COP_{77K} = 0.054; COP_{200K} = 0.38).

[b]Energy efficiency is estimated based on the total energy consumption of each H_2 delivery mode at the terminal and for a H_2 energy content of 120 MJ/kg H_2.

Table S5 Energy requirements (in GJ) of H_2 delivery modes for H_2 distribution to refueling stations for 50,000 kg/day (excludes energy costs of storage at refueling stations).

	Comp-H_2 Gas Terminal – Distribution						
	Comp-H_2 350 bar	Comp-H_2 500 bar	Liq-H_2	Ni_2(*m*-dobdc) (200 K)	MOF-5 (200 K)	Ni_2(*m*-dobdc) (77 K)	MOF-5 (77 K)
Compression							
(1) Cooling Energy	266	330	NA	152	152	254	254
(2) Refrigeration –Power[a]	NA	NA	NA	400	400	4704	4704
(3) Electricity	275	243	NA	80	80	87	87
Adsorption							
(4) Cooling Energy	NA	NA	NA	307	100	307	100
(5) Refrigeration –Power[a]	NA	NA	NA	808	263	5685	1852
Tube Precooling							
(6) Cooling Energy	NA	NA	NA	452	421	47	17
(7) Refrigeration –Power[a]	NA	NA	NA	1,189	1,108	870	315
Liquefaction							
(8) Electricity	NA	NA	1,651	NA	NA	NA	NA
	Refueling Station – Distribution						
Compression							
(9) Electricity	NA	NA	NA	648	802	214	617
(10) Cooling Energy	NA	NA	NA	570	724	50	452
Total Energy Consumption	541	573	1,651	3,695	3,377	11,610	8,027
	(1+2)	(1+2)	(8)	(2+3+5+7+9+10)	(2+3+5+7+9+10)	(2+3+5+7+9+10)	(2+3+5+7+9+10)
Share of energy costs at gas terminal in total delivered H_2 energy content[b]	9%	10%	28%	62%	56%	194%	134%

[a]Refrigeration power requirements for the MOF-H_2 systems is estimated based on the cooling energy consumption divided over the COP value (COP77K = 0.054; COP200K = 0.38).

[b]Energy efficiency is estimated based on the total energy consumption of each H_2 delivery mode at the terminal and for a H_2 energy content of 120 MJ/kg H_2.

1.4.2 Capital Costs

Capital costs for the gas terminal equipment, truck cabs, and trailers are included in Table S6. The tube cost of both Comp-H_2 (tank type IV) and MOF–H_2 systems (tank type III) is estimated based on the operating pressure by employing the "tankinator" Excel file which is developed by PNNL[10,32] We assume the MOF material can be employed for 5,000 adsorption cycles (5,000 roundtrips) in our base case. When the MOF material is replaced, it is not easily recovered from the trailer. Therefore, we estimate the trailer lifespan based on the specified number of cycles required per year for trucks in each supply chain scenario.

The levelized cost of H_2 is estimated on an annual basis, assuming a 357-day availability. We then model capital and operating costs over a time period of 30 years. The levelized H_2 cost for all studied delivery schemes is estimated according to Eq. S12.

$$\text{Levelized } H_2 \text{ Cost} = \frac{Capital\_Costs_{PV} \cdot FCR}{\text{Annual } H_2 \text{ Capacity}} + \frac{\text{Annual O\&M Costs}}{\text{Annual } H_2 \text{ Capacity}} \quad \text{(S12)}$$

where $Capital\_Cost_{PV}$ = present value of capital costs; Annual O&M = Annual Operating and Maintenance Costs; Annual H_2 Capacity = Daily H_2 capacity × 357 days; and FCR=fixed charge rate given by Eq. S13 and Eq. S14:[4,33]

$$\text{FCR} = CRF \cdot \frac{(1 - Tax \cdot D_{PV})}{(1 - Tax)} \quad \text{(S13)}$$

$$Capital\ Recovery\ Factor = CRF = \frac{i \cdot (1 + i)^n}{((1 + i)^n - 1)} \quad \text{(S14)}$$

where n = project lifetime (in years); Tax = total tax rate; D_{pv} = present value of depreciation; and i = real discount rate (%).

The cost values employed in this technoeconomic model are presented in Table S6.

Table S6 Economic parameters considered for the studied H_2 delivery technologies for 50,000 kg H_2/day.

Model Parameter	Base Case Value & Reference
Compressor size	35 kg/h
Compressor system cost (Comp-H_2-350 bar)*	\$60,855,860 [34]
Compressor system cost (Comp-H_2-500 bar)*	\$64,058,239 [34]
Compressor system cost (MOFs)*	\$54,106,083 [34]
Refrigerator system cost (Ni_2(*m*-dobdc) 200 K)*	\$23,608,137 [34]
Refrigerator system cost (Ni_2(*m*-dobdc) 77 K)*	\$147,340,764 [34]
Refrigerator system cost (MOF-5 200 K)*	\$23,069,696 [34]
Refrigerator system cost (MOF-5 77 K)*	\$146,742,651 [34]
Compressor & refrigerator lifetime	15 years [4]
Compressor & refrigerator depreciation time	10 years
Liquefier cost	\$144,060,275 [4]
Liquefier lifetime	30 years [9]
Liquefier depreciation time	15 years
Truck lifetime	5 years [4]
Truck depreciation time	3 years
Trailer lifetime	Defined by MOF cycles
Trailer depreciation time	3 years
Storage tank lifetime	30 years[9]
Storage tank depreciation time	15 years[4]
Labour cost	\$29/h [35]
Truck cost	\$145,281 [36]
Trailer cost (excl. tubes)	\$96,854[36]
MOF cost	\$10/kg [37]
Electricity Cost	\$0.069/kwh [38]
Refrigeration water (278.15 → 288.15 K)	\$4.43/GJ
Fuel cost	\$3.29/gallon [38]
Fuel efficiency	11 km/gallon [39]
Inflation rate	1.9% [4]
Real discount rate	10%[4]
Total tax rate	38.9% [4]
Insurance, permits & licenses	\$0.061/km
Maintenance & repairs	\$0.104/km
Tolls	\$0.017/km
Tires	\$0.024/km
Boil-off H_2 losses	0.5%
Liquefier H_2 losses	0.5%
Liquid terminal H_2 losses during loading	0.5%
Compressor H_2 losses	0.5%
CPI (2020; 2016; 2014, 2007; 1998)	263.1; 240.1; 236.7; 207.3; 163

*Refrigerator system refers to transmission supply chain and comprises multiple refrigerators with size and cost estimated based on the equation provided in Towler and Sinnott.[34]

2. Breakthrough Curve Analysis

Based on the adsorption model in Section 1.2, we generated breakthrough curves (Fig. 1, main text; Fig. S4) that allowed us to estimate the amount of adsorbent, H_2 adsorbed and desorbed per tube, as well charging and discharging times for the MOFs (Table S7). In the absence of experimentally determined Peclet numbers for the examined MOF-H_2 systems at the selected operating conditions, empirical correlations have been employed, as shown in Eqs. S14-S16.[40,41] In order to capture the effect of the Peclet number on the adsorption performance , a Pe ≈ 1 (Eq.S15), Pe < 1 (S16), and Pe > 1 (Eq. S17) were selected to model the base case, low-packing density, and high packing density scenarios, respectively.

$$\frac{1}{\mathrm{Pe}} = \frac{0.65}{1 + 7\sqrt{\varepsilon_b/(\mathrm{Re} \times \mathrm{Sc})}} + \frac{0.67\varepsilon_b}{\mathrm{Re} \times \mathrm{Sc}} \qquad \text{(S15)}$$

$$\mathrm{Pe} = \frac{0.7D_m}{D\mathrm{p}} + \frac{1}{0.4 + 1.76D_m/(D\mathrm{p} \times \frac{u}{2})} \qquad \text{(S16)}$$

$$\mathrm{Pe} = 71.86(1 - \varepsilon_b)^{0.67}\mathrm{Re}^{0.23} \qquad \text{(S17)}$$

where Re is the Reynolds number given by $\mathrm{Re} = D_p \times u \times \rho/(\mu \times \varepsilon_b)$,

u is the gas velocity, ρ is gas density, and μ is gas dynamic viscosity,

Sc is Schmidt number defined as $\mathrm{Sc} = \mu/(\rho \times D_m)$,

D_p is particle diameter, and

D_m is the molecular diffusion coefficient which is defined to be 2.4×10^{-5} cm²/s[42] and 1.63×10^{-4} cm²/s[43] at 77 and 200 K, respectively. The selected diffusion coefficients are assumed to be applicable to 100 bar.

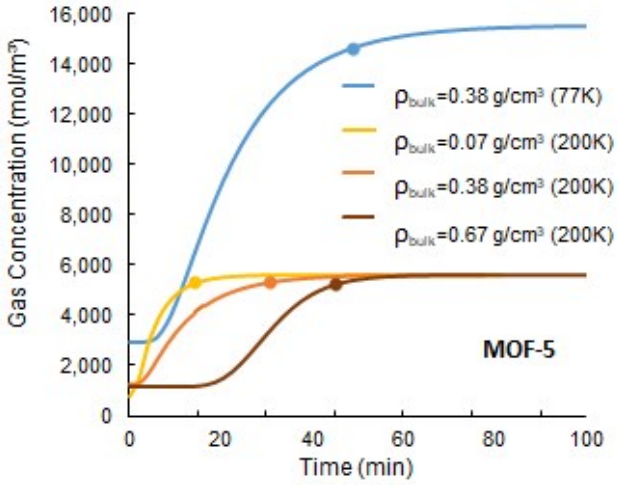

Fig. S4 Simulated gas-phase concentration breakthrough curves for H_2 adsorption in MOF-5, where filled circles indicate 95% saturation achieved. Initial non-zero concentrations at t = 0 denote that the tubes are not fully emptied during discharge cycles.

Table S7 Adsorption and desorption process parameters (values per tube; 9 tubes per truck).

System	Adsorbent mass (kg)	H_2 mass (kg)	Charging time (min)	Desorption pressure (bar)	H_2 desorbed (kg)	Desorption time (min)
Base case: ε_b = 0.6 and ε_p = 0.2 ($\rho_{bulk\_MOF\text{-}5}$ = 0.19 g/cm³; $\rho_{bulk\_Ni2(m\text{-}dobdc)}$ = 0.38 g/cm³) (Peclet number estimated based on Eq. S14)						
Ni_2(*m*-dobdc) (200 K)	820	7.2	37	3.4	2.4	52
Ni_2(*m*-dobdc) (77 K)	820	33	50	6.3	16.5	50
MOF-5 (200 K)	417	6.8	31	2.0	1.8	24
MOF-5 (77 K)	417	35.2	49	1.0	22.9	59
Low packing density variation: ε_b = 0.7 and ε_p = 0.8 ($\rho_{bulk\_MOF\text{-}5}$ = 0.04 g/cm³; $\rho_{bulk\_Ni2(m\text{-}dobdc)}$ = 0.07 g/cm³) (Peclet number estimated based on Eq. S15)						
Ni_2(*m*-dobdc) (200 K)	154	3.3	16	1.9	0.6	30
Ni_2(*m*-dobdc) (77 K)	154	20.1	31	1.2	6.3	31
MOF-5 (200 K)	78	3.4	14	1.0	0.4	11
MOF-5 (77 K)	78	20.1	34	3.0	5.0	26
High packing density variation: ε_b = 0.3 and ε_p = 0.2 ($\rho_{bulk\_MOF\text{-}5}$ = 0.34 g/cm³; $\rho_{bulk\_Ni2(m\text{-}dobdc)}$ = 0.67 g/cm³) (Peclet number estimated based on Eq. S16)						
Ni_2(*m*-dobdc) (200 K)	1436	17.1	49	3.1	9.7	68
Ni_2(*m*-dobdc) (77 K)	1436	51.6	45	3.9	40.8	46
MOF-5 (200 K)	730	17.1	45	1.7	11.7	52
MOF-5 (77 K)	730	52.4	47	1.2	41.8	45

3. Additional Sensitivity Analyses

3.1 Market Size

The impact of the H_2 delivery rate on the transmission cost was studied for the range of 2,000–120,000 kg H_2/day. As can be seen in Fig. S5 (upper), as the delivered H_2 is increased from 2,000 to 20,000 kg H_2 per day, the cost of the MOF systems drops by 1–2% (from starting costs of \$17.7 or \$10.2 and \$23.9 or \$7.5/kg H_2, for Ni_2(*m*-dobdc) and MOF-5 at 200 or 77 K, respectively). For larger delivery rates, the transmission cost in each case is relatively constant, as indicated by the plateau of the respective cost curves. This behavior provides important insights into the operating window for which economies of scale can be attained for the MOF–H_2 systems, given the considerations and assumptions made in this TEA.

At a delivery rate of 2,000 kg H_2/day, the transmission cost for Comp-H_2 is \$2.1/kg for both 350 and 500 bar systems; if the delivery rate is increased to 30,000 kg/day, the cost decreases by 13 and 15%, respectively. In contrast, the transmission cost of Liq-H_2 decreases by 37% upon increasing the delivery rate from 2,000 and 50,000 kg H_2/day. Regardless of examined capacity (H_2 "demand"), the relative cost of the MOF–H_2 systems compared to that of the conventional H_2 delivery modes remains approximately the same.

The distribution cost profile of the MOF–H_2 systems (Fig. S5, lower) is again relatively constant with increasing H_2 delivery rate, decreasing by 1–2% from 2,000 to 120,000 kg H_2/day. The Comp-H_2 systems at 350 and 500 bar demonstrate a maximum reduction of 7% and 6% in their distribution costs, respectively, as the daily H_2 demand rate increases from 2,000 to 120,000 kg H_2/day. The cost of Liq-H_2

delivery decreases by 43% when the H_2 demand increases from 2,000 to 120,000 kg per day, resulting in a minimum distribution cost \$3.6/kg H_2 which is 25 and 12% lower than the 350 and 500 bar Comp-H_2 systems, respectively.

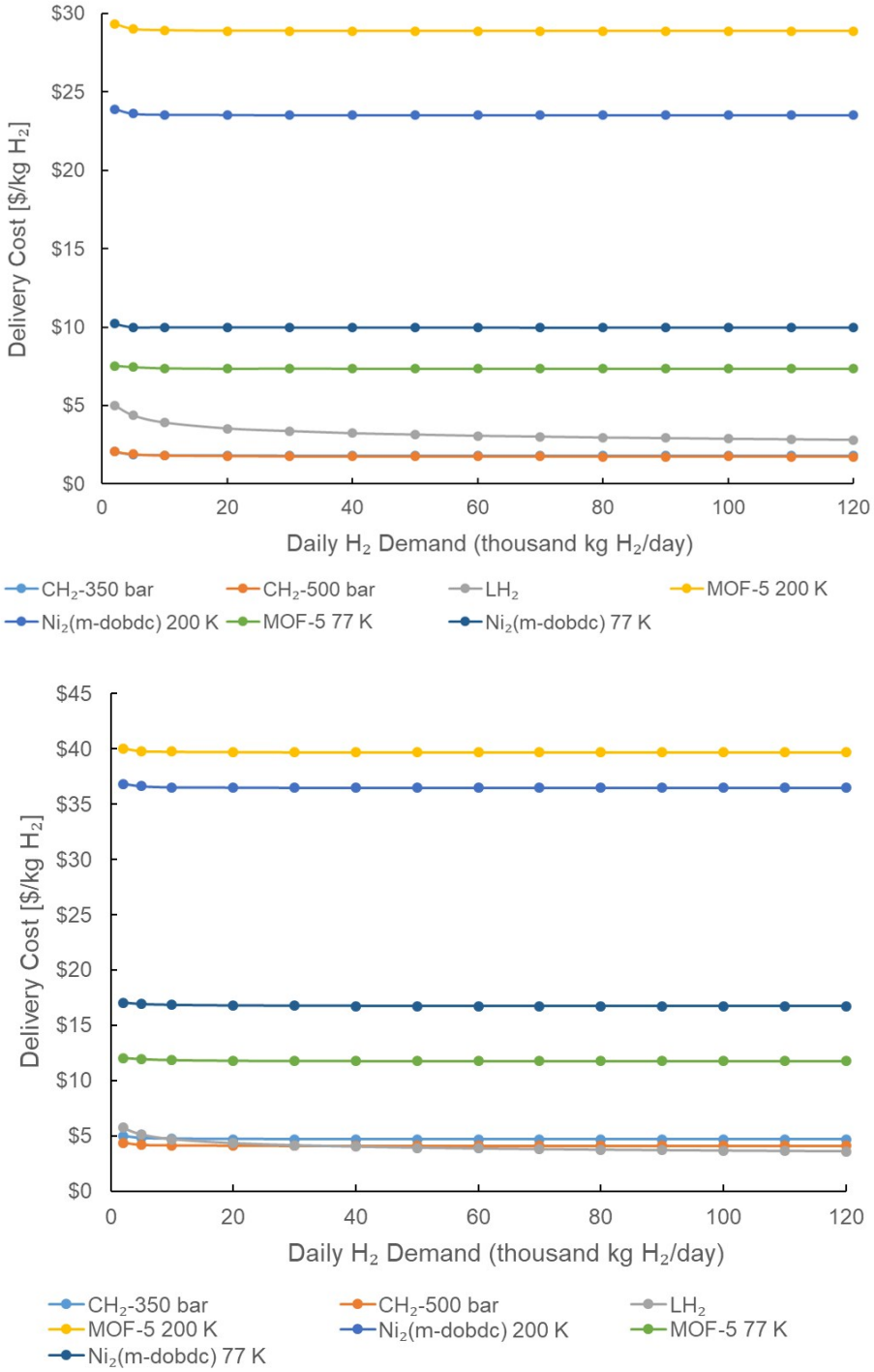

Fig. S5 Sensitivity analysis showing the effect of H_2 daily demand (used as a proxy for market size) on (upper) H_2 transmission (long distance, point-to-point) and (lower) H_2 distribution (short distance, city-gate to refueling stations) delivery costs for all examined H_2 delivery technologies. Technologies include

Comp-H_2 trucks, Liq-H_2 trucks, and adsorption-based MOF trucks employing the assumptions of the base case (see Table S7).

3.2 Parameter Variation and Cost Boundaries

Both "minimum" and "maximum" cost scenarios for transmission, distribution, and transmission-distribution were determined for the MOF–H_2 systems. Minimum costs for the MOF–H_2 systems were derived assuming the high packing density case (see Table S7), a cost of $5/kg MOF pellets, driverless trucks, and MOF stability to 15,000 cycles; maximum costs were determined assuming a low packing density (Table S7), a cost of $15/kg MOF pellets, and MOF stability for 5,000 adsorption cycles. The resulting costs are presented in Table S8.

Table S8 Costs associated with minimum and maximum scenarios for H_2 transmission, distribution and transmission/distribution for MOF–H_2 delivery technologies for 50,000 kg H_2/day, expressed in $/kg H_2.

Material	Transmission		Distribution		Transmission-distribution	
	Minimum	Maximum	Minimum	Maximum	Minimum	Maximum
Ni_2(*m*-dobdc) (200 K)	4.0	81.7	9.2	81.0	10.5	109.2
MOF-5 (200 K)	3.3	119.3	8.6	109.2	10.1	167.0
Ni_2(*m*-dobdc) (77 K)	7.3	14.3	9.1	20.6	8.1	30.3
MOF-5 (77 K)	5.7	14.6	7.3	28.1	8.0	32.2
Comp-H_2-350 bar	1.4	NA	4.5	NA	4.8	NA
Comp-H_2-500 bar	1.4	NA	4.0	NA	4.3	NA
Liq-H_2	3.1	NA	3.9	NA	4.1	NA

3.3 MOF–H_2 versus Comp-H_2 (Variable Operating Pressures)

The H_2 uptake capacity of the Ni_2(*m*-dobdc) and MOF-55 adsorption systems has been evaluated for a set of operating pressures at 77 K, and two different packing densities. The performance of the given system has been compared with that of the Comp-H_2, assuming that the latter occupies the same volume as that of the Ni_2(*m*-dobdc) and MOF-5 packed bed. For all the examined pressures, as shown in Table S9 and S10, the H_2 uptake achieved with both MOF systems is larger than with Comp-H_2. However, the gravimetric capacities of both MOF systems are far lower than that of the Comp-H_2 system overall (except at 1 bar), due to the mass of the adsorbent. It is important to mention that the values obtained at pressures higher than 100 bar have been extrapolated from the same isotherm equation employed in this analysis, and thus their validity needs to be assessed based on relevant experimental data.

Table S9 H_2 storage capacity of the Ni_2(*m*-dobdc) and Comp-H_2 systems at 77 K and different operating pressures.

Ni_2(*m*-dobdc)–H_2 System (high packing density, 0.67 g/cm^3)					
Pressure (bar)	**1**	**50**	**100**	**300**	**500**
H_2 uptake (kg)	1.1	31.6	59.6	115.0	138.0
Adsorbent mass (kg)[a]	1,436	1,436	1,436	1,436	1,436
Tank weight (kg)[b]	269	269	407	1,222	2,116
MOF-bed volume (m^3)	2.15	2.15	2.15	2.15	2.15
Gravimetric capacity (wt %)[c]	0.1%	1.8%	3.1%	4.1%	3.7%
Ni_2(*m*-dobdc)–H_2 System (low packing density, 0.07 g/cm^3)					
Pressure (bar)	**1**	**50**	**100**	**300**	**500**
H_2 uptake (kg)	0.3	13.5	25.7	49.0	58.9
Adsorbent mass (kg)[a]	154	154	154	154	154
Tank weight (kg)[b]	269	269	407	1,222	2,116
MOF-bed volume (m^3)	2.16	2.16	2.16	2.16	2.15
Gravimetric capacity (wt %)[c]	0.1%	3.1%	4.4%	3.4%	2.5%
Comp-H_2					
Pressure (bar)	**1**	**50**	**100**	**300**	**500**
H_2 uptake (kg)	1.0	52.4	99.0	184.3	220.3
Tank weight (kg)[d]	179.8	179.8	277.4	677.8	1058.5
Gravimetric capacity (wt %)[e]	0.5%	22.6%	26.3%	21.4%	17.2%

[a]Adsorbed amount estimated for an empty tank.

[a] Tank weight estimated for a type III tank[10] given a 12.19 m tube length, 0.56 m tube diameter, and given tube pressure.

[b] Gravimetric capacity: H_2 uptake/(H_2 uptake + Adsorbent mass + Tank weight).

[c] Tank weight estimated for a type IV tank[10] given a 12.19 m tube length, 0.56 m tube diameter, and given tube pressure.

[d] Gravimetric capacity: H_2 uptake/(H_2 uptake + Tank weight).

Table S10 H_2 storage capacity of the MOF-5 and Comp-H_2 systems at 77 K and different operating pressures.

MOF-5–H_2 System (high packing density, 0.34 g/cm^3)					
Pressure (bar)	**1**	**50**	**100**	**300**	**500**
H_2 uptake (kg)	0.8	31.7	59.7	115.2	138.2
Adsorbent mass (kg)[a]	730	730	730	730	730
Tank weight (kg)[b]	269	269	407	1,222	2,116
MOF-bed volume (m^3)	1.5	1.5	1.5	1.5	1.5
Gravimetric capacity (wt %)[c]	0.1%	3.1%	5.0%	5.6%	4.6%
MOF-5–H_2 System (low packing density, 0.04 g/cm^3)					
Pressure (bar)	**1**	**50**	**100**	**300**	**500**
H_2 uptake (kg)	0.3	13.7	25.4	49.7	59.8
Adsorbent mass (kg)[a]	78.0	78.0	78.0	78.0	78.0
Tank weight (kg)[b]	268.6	268.6	407.3	1222.1	2116.2
MOF-bed volume (m^3)	0.2	0.2	0.2	0.2	0.2
Gravimetric capacity (wt %)[c]	0.1%	3.8%	5.0%	3.7%	2.7%
Comp-H_2					
Pressure (bar)	**1**	**50**	**100**	**300**	**500**
H_2 uptake (kg)	0.5	26.6	50.3	93.7	112.0
Tank weight (kg)[d]	179.8	179.8	277.4	677.8	1058.5
Gravimetric capacity (wt %)[e]	0.3%	12.9%	15.4%	12.1%	9.6%

[a]Adsorbed amount estimated for an empty tank.

[a] Tank weight estimated for a type III tank[10] given a 12.19 m tube length, 0.56 m tube diameter, and given tube pressure.

[b] Gravimetric capacity: H_2 uptake/(H_2 uptake + Adsorbent mass + Tank weight).

[c] Tank weight estimated for a type IV tank[10] given a 12.19 m tube length, 0.56 m tube diameter, and given tube pressure.

[d] Gravimetric capacity: H_2 uptake/(H_2 uptake + Tank weight).

3.4 Combined Transmission & Distribution Supply Chain Cost Analysis

The cost profile of the combined transmission-distribution delivery scenario, as shown in Figs. S6 (for Comp-H_2 = CH_2) and Liq-H_2 = LH_2)) and Fig. S7 (MOF–H_2), is dominated by the "last-mile" costs, particularly those associated with the refueling stations. For the MOFs at 77 K, the levelized cost of the trucks is quite low compared with the levelized cost of the refueling stations. In the case of MOF-5 and Ni_2(*m*-dobdc)-H_2 systems at 200 K, the levelized costs are \$50.1 and \$43.6/kg H_2, respectively, and in both cases, refueling station costs constitute the greatest percentage of the total, 32% and 37% respectively. The levelized delivery cost for the 77 K MOF-5 system is \$13.4/kg H_2, whereas for the 77 K Ni_2(*m*-dobdc) system the cost is \$18.4/kg H_2. Increasing the total distance from 101 to 150 km increases the delivery cost of the selected MOF–H_2 systems by 5 to 18%, suggesting a combined transmission-distribution delivery scenario is quite sensitive to geographic conditions.

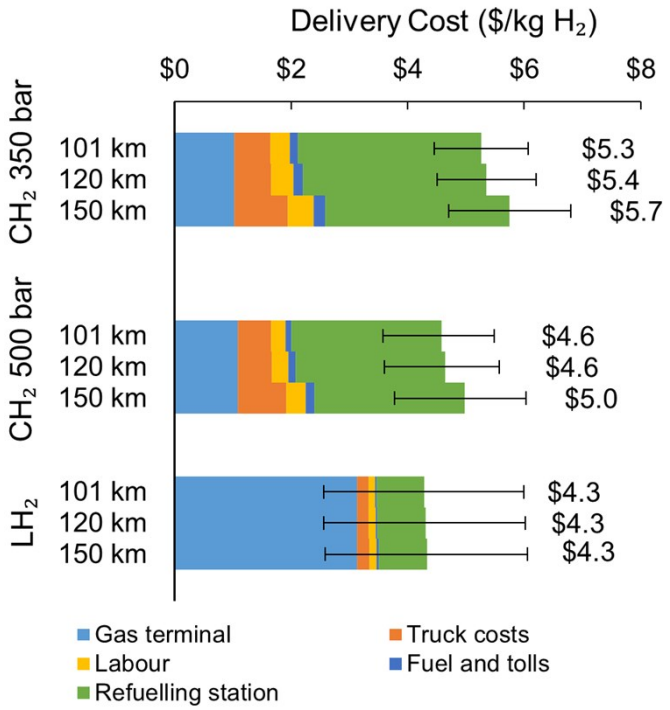

Fig. S6 Levelized delivery cost for incumbent Comp-H_2 (CH_2) and Liq-H_2 (LH_2) technology supply chains where transmission and distribution are served by one truck fleet for 50,000 kg H_2/day (100 km from gas terminal to city gate; 1 km from city gate to refueling station). Error bar lower bounds reflect a 50% decrease in input capital and operating costs. Error bar upper bounds reflect a 50% increase in the input capital and operating cost values.

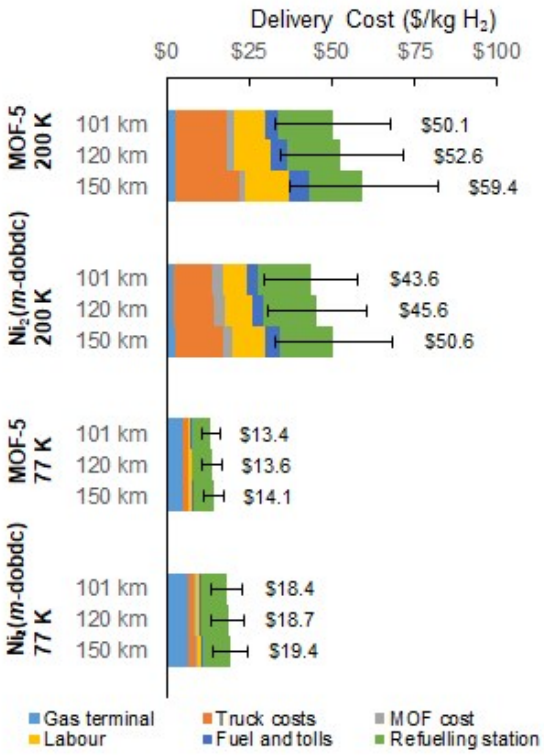

Fig. S7 Levelized delivery cost for MOF-based supply chains where transmission and distribution are served by one truck fleet for 50,000 kg H_2/day (100 km from gas terminal to city gate; 1 km from city gate to refueling station). Error bar lower bounds reflect a 50% decrease in input capital and operating costs and an assumption that tube trailers can be pre-cooled from an initial temperature of 87 K. Error bar upper bounds reflect a 50% increase in the input capital and operating cost values and "cold start-up" where tube trailers must be pre-cooled from an initial temperature of 298 K.

4. Model Benchmarking

Our model was benchmarked by comparing the estimates of levelized cost of H_2 delivery, as well as model derived characteristics of supply chain components, with outputs generated for the same supply chain conditions using HDSAM. According to HDSAM, the transmission-distribution cost of the Comp-H_2-500 bar system for 50,000 kg H_2/day, transmission distance of 100 km and distribution distance of 10 km (city area of 17 mi^2 in HDSAM model) — excluding geological storage and pipeline transmission — is estimated at \$4.5/kg H_2 (\$2020), wherein \$1.2, \$0.8, and \$2.5 are allocated to the gas terminal, truck and refueling station, respectively. A transmission-distribution cost of \$4.6/kg H_2 was estimated in this study, and there is a 9%, 15%, and 2% difference in the aforementioned cost components. For the gas terminal, the difference lies in additional auxiliary equipment and operating costs (e.g., pumps, pipeline, land, and labor costs) that were included in HDSAM but not in this study. The HDSAM uses a different method for estimating the number of cabs and trailers, and assumes a fraction of trailers are on reserve. The overall 2% difference in the total distribution cost, and our ability to pinpoint sources of cost differences, renders the two models comparable and enhances the reliability of the presented results for adsorption-based technologies.

5. Performance of Ni_2(*m*-dobdc)–H_2 system at ambient temperature

The performance of the Ni_2(m-dobdc)–H_2 system, operated at 298 K and 250 bar, was been evaluated for the three different supply chains (transmission, distribution, and transmission-distribution) based on the assumptions made in the base case scenario. The same adsorption model presented in Section 1.2 was employed in this test case study, assuming the same molecular diffusion coefficient (D_m) value used for the Ni_2(m-dobdc)-H_2 system at 200 K and 100 bar. The adsorbed and desorbed amount is estimated at 10.7 kg H_2/tube and 3.4 kg H_2/tube, respectively, while the desorption pressure is set at 1.1 bar. Due to the higher operating pressure of 250 bar, the same storage pressure as assumed for the Comp-H_2 refueling station system (430 bar) is considered in this case. The cooling requirements of the system have been assumed to be covered by the refrigeration water reported in Table S6.

As shown in Figure S8, Increasing the transmission distance from 25 to 300 km results in a 170% increase of the delivery cost of H_2 using Ni_2(*m*-dobdc) at ambient temperature and high pressure. The distribution cost profile is primarily dominated by the refueling station and truck costs, with a respective share in the range of 46 to 48% and 30 to 33% for the examined distances. For the combined transmission-distribution delivery scenario exhibits a similar trend, with the delivery cost increasing by 11% when the traveled distance is increased from 101 to 150 km.

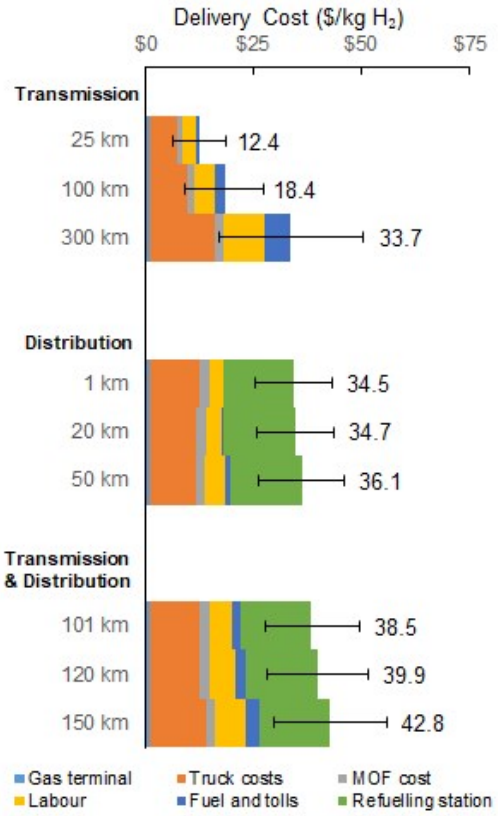

Fig. S8 Levelized delivery cost for Ni_2(*m*-dobdc)-based supply chains where transmission and distribution are served by one truck fleet for 50,000 kg H_2/day (100 km from gas terminal to city gate; 1 km from city gate to refueling station). Error bar lower bounds reflect a 50% decrease in input capital and operating costs Error bar upper bounds reflect a 50% increase in the input capital and operating cost values.

6. Effect of particle size on adsorption/desorption efficiency

Adsorbent particle size is an important parameter affecting the dispersion and diffusion mechanisms of a gas/liquid-solid adsorption system.[44] In the absence of an experimental system that can provide information on mass transfer phenomena, the model adopted in this study for the MOF–H_2 systems considers only the axial dispersion, which is described by the Peclet number, and no mass transfer limitations. We have carried out an additional analysis of the effect of larger particle size, 1 mm, on the efficiency of H_2 adsorption and desorption in the MOF-based systems.

Comparing data for the same mass of 1 µm particles (Table S7) and 1 mm particles (Table S11), in the case of the 200 K Ni_2(*m*-dobdc) and MOF-5 systems, the larger particle size yields a 54% and 67% higher quantity of desorbed H_2. However, at 77 K, the quantity of H_2 that can be desorbed from 1 mm particles of Ni_2(*m*-dobdc) and MOF-5 is 50% and 53% *lower*, respectively, than the desorbed amount from the 1 µm particles at the same temperature. The change in the adsorption/desorption performance of the MOF systems with larger particle size can be attributed to changes in the Peclet number, which is estimated in this study from the Re number, which is derived from particle size, gas velocity, and physical properties at the studied conditions, as described in Eqs. S14–S16. At 200 K, the Peclet number for the 1 mm particles is higher than the 1 µm particles under the same conditions, denoting a lower degree of axial dispersion, and resulting in sharper breakthrough curves,[45–47] whereas at 77 K the Peclet number is smaller than in the corresponding base case, reflecting higher dispersion.[48]

Although particle size has been shown to influence the Peclet number, it is important to consider this effect along with the effect on mass transfer mechanisms in order to assess the magnitude of impact on the overall adsorption efficiency. Research has shown that smaller particle size provides higher surface area and increases mass transfer rate, which enhances adsorption capacity.[45–47] However, batch experimental data, obtained from measurements on a MOF in powder form, may not provide accurate insights for large scale fixed-bed systems, which are relevant in process modeling for predicting adsorption performance at scale-up conditions.[49] Specifically, the design of larger particles and pellets, as sometimes employed in industrial applications, leads to uncertain losses in the MOF adsorption capacity due to degradation of the physical and chemical properties of the initial powder.[50–52] As such, additional experimental data is necessary for robust modeling of the adsorption system at scaled-up conditions to better understand the prevailing mass and heat transfer phenomena. For this reason, we use a simplified model to bound the effect of design parameters on adsorption/desorption efficiency.

Table S11 Adsorption and desorption process parameters for a MOF particle size of 1 mm and the same operating conditions as in the base case (values per tube; 9 tubes per truck).

System	Adsorbent mass (kg)	H_2 mass (kg)	Charging time (min)	Desorption pressure (bar)	H_2 desorbed (kg)	Desorption time (min)
ε_b = 0.6 and ε_p = 0.2 ($\rho_{bulk\_MOF\text{-}5}$ = 0.19 g/cm^3; $\rho_{bulk\_Ni2(m\text{-}dobdc)}$ = 0.38 g/cm^3) (Peclet number estimated based on Eq. S14)						
Ni_2(*m*-dobdc) (200 K)	820	9.3	50	3.9	3.7	43
Ni_2(*m*-dobdc) (77 K)	820	23.3	37	4.6	8.3	39
MOF-5 (200 K)	417	9.0	40	2.5	3.0	32
MOF-5 (77 K)	417	24.9	39	0.2	10.8	52

7. References

1 M. T. Kapelewski, T. Runčevski, J. D. Tarver, H. Z. H. Jiang, K. E. Hurst, P. A. Parilla, A. Ayala, T. Gennett, S. A. Fitzgerald, C. M. Brown and J. R. Long, *Chem. Mater.*, 2018, **30**, 8179–8189.

2 S. S. Kaye, A. Dailly, O. M. Yaghi and J. R. Long, *J. Am. Chem. Soc.*, 2007, **129**, 14176–14177.

3 R. Sathre, B. Greenblatt, R. Sathre, C. D. Scown, W. R. Morrow, J. C. Stevens, I. D. Sharp, J. W. Ager, K. Walczak, A. Houle and B. Greenblatt, *Energy Environ. Sci.*, 2014, **7**, 3264–3278.

4 Argonne National Laboratory, Hydrogen Delivery Scenario Analysis Model (HDSAM), https://hdsam.es.anl.gov/index.php?content=hdsam.

5 Ballard Power Systems and Nel Hydrogen, *Hydrogen at Scale for Fuel Cell Electric Buses A California Case Study*, 2019.

6 California Energy Commission, *Joint Agency Staff Report on Assembly Bill 8: Assessment of Time and Cost Needed to Attain 100 Hydrogen Refueling Stations in California*, 2015.

7 California Fuel Cell Partnership, What Do You Need To Know About Hydrogen Fueling Operations?, https://cafcp.org/sites/default/files/Stations-Fact-sheet3_0.pdf.

8 Argonne National Laboratory, Hydrogen Refueling Station Analysis Model (HRSAM), https://hdsam.es.anl.gov/index.php?content=hrsam.

9 US Department of Energy, DOE Technical Targets for Hydrogen Delivery, https://www.energy.gov/eere/fuelcells/doe-technical-targets-hydrogen-delivery.

10 Hydrogen Storage Engineering Center of Excellence (HSECoE, Tankinator, http://hsecoe.org/models.html.

11 C. Yang and J. Ogden, *Int. J. Hydrogen Energy*, 2007, **32**, 268–286.

12 Inc City Machine & Welding, Hydrogen Tube Trailer -9 Tubes DOT 3AAX 2400 PSI 40 FT, https://cmwelding.com/configuration/hydrogen-h2-tube-trailer-9-tubes-dot-3aax-2400psi-40-ft.

13 US Department of Transportation, *Freight Management and Operations*, 2017.

14 The MathWorks, Inc.MATLAB and Statistics Toolbox Release 2018b.

15 M. M. Dubinin, in *Progress in Surface and Membrane Science*, eds. D. A. Cadenhead, J. F. Danielli and M. D. Rosenberg, Academic Press, New York, 1975, vol. 9, pp. 1–70.

16 M. M. Dubinin and A. V. Astakhov, *Izv. Akad. Nauk SSSR, Ser. Khim*, 1971, **5**, 17.

17 M. Duquesne, J. Toutain, A. Sempey and E. Palomo, 2014, **71**, 469–480.

18 S. Saha, U. Sarkar and S. Mondal, *Desalin. Water Treat. ISSN*, 2012, **37**, 277–287.

19 K. S. Hwang, D. K. Choi, S. Y. Gong and S. Y. Cho, *Chem. Eng. Sci.*, 1997, **52**, 1111–1123.

20 A. S. Yusuff, L. T. Popoola, O. O. Omitola, A. O. Adeodu and I. A. Daniyan, 2013, **4**, 811–822.

21 R. Perry, D. Green and J. Maloney, *Perry's chemical engineers' handbook*, 1997.

22 C. C. Rodrigues and D. Moraes, *Adsorpt. Sci. Technol.*, 2002, **20**, 1013–1022.

23 L. C. S. D. Krishnaiah, S.M. Anisuzzaman, C.G. Joseph, S. Abang, *J. Appl. Sci., 14*, 2014, **14**, 3249-3255.

24 M. Andrea, E. De Franco, C. B. De Carvalho, M. M. Bonetto, R. D. P. Soares and L. A. F, *J. Clean. Prod.*, 2017, **161**, 947–956.

25 R. Lakshmipathy and N. C. Sarada, *Environ. Sci. Water Res. Technol.*, 2015, **1**, 244–250.

26 L. Li, Z. Sun, H. Li and T. C. Keener, *J. Air Waste Manage. Assoc.*, 2012, **62**, 1196–1202.

27 M. T. Kapelewski, S. J. Geier, M. R. Hudson, D. Stück, J. A. Mason, J. N. Nelson, D. J. Xiao, Z. Hulvey, E. Gilmour, S. A. Fitzgerald, M. Head-Gordon, C. M. Brown and J. R. Long, *J. Am. Chem. Soc.*, 2014, **136**, 12119–12129.

28 B. Schmitz, U. Müller, N. Trukhan, M. Schubert, G. Férey and M. Hirscher, *ChemPhysChem*, 2008, **9**, 2181–2184.

29 W. Plazinski, *Adsorption*, 2013, **19**, 659–666.
30 F. A. Kloutse, R. Zacharia, D. Cossement and R. Chahine, *Microporous Mesoporous Mater.*, 2015, **217**, 1–5.
31 D. R. Ladner, *Cryocoolers*, 2011, **16**, 633–644.
32 E. Rivard, M. Trudeau and K. Zaghib, *Materials (Basel).*, 2019, **12**, 1–22.
33 C. Mone, T. Stehly, B. Maples and E. Settle, *2014 Cost of Wind Energy Review*, 2015.
34 G. Towler and R. K. Sinnott, *Chemical Engineering Design-Principles, Practice and Economics of Plant and Process Design*, Butterworth-Heinemann, 2nd edn., 2012.
35 United States Department of Labor, *TED:The Economics Daily*, 2019.
36 W. A. Amos, *Costs of Storing and Transporting Hydrogen Costs of Storing and Transporting Hydrogen*, 1998.
37 B. D. James, *2015 DOE Hydrogen and Fuel Cells Program Review-Hydrogen Storage Cost Analysis*, 2015.
38 U.S. Energy Information Administration, *Short-Term Energy Outlook*, 2019.
39 US Department of Energy, *Average Fuel Economy of Major Vehicle Categories*, 2018.
40 S. Omid and T. Gu, *J. Chromatogr. A*, 2017, **1490**, 133–137.
41 Y. Jin and F. Wei, *Multi-phase chemical reaction engineering and technology*, Tsinghua University Press, 2006.
42 D. Saha, Z. Wei and S. Deng, *Sep. Purif. Technol.*, 2009, **64**, 280–287.
43 K. Koizumi, K. Nobusada and M. Boero, *Phys. Chem. Chem. Phys.*, 2019, **21**, 7756–7764.
44 P. S. Pauletto, G. L. Dotto and N. P. G. Salau, *Chem. Eng. Res. Des.*, 2020, **157**, 182–194.
45 A. Lisowski, P. Matkowski, M. Dąbrowska, M. Piątek, A. Świętochowski, J. Klonowski, L. Mieszkalski and V. Reshetiuk, *Waste and Biomass Valorization*, 2020, **11**, 63–75.
46 P. Suresh Kumar, L. Korving, K. J. Keesman, M. C. M. van Loosdrecht and G. J. Witkamp, *Chem. Eng. J.*, 2019, **358**, 160–169.
47 R. Kumari and S. Dey, *Int. J. Phytoremediation*, 2019, **21**, 1263–1271.
48 P. Sridhar, N. V. S. Sastri, J. M. Modak and A. K. Mukherjee, *Chem. Eng. Technol.*, 1994, **17**, 422–429.
49 M. R. Samarghandi, M. Hadi and G. McKay, *Adsorpt. Sci. Technol.*, 2014, **32**, 791–806.
50 B. P. Prajwal and K. G. Ayappa, *Adsorption*, 2014, **20**, 769–776.
51 N. Chanut, A. D. Wiersum, U. H. Lee, Y. K. Hwang, F. Ragon, H. Chevreau, S. Bourrelly, B. Kuchta, J. S. Chang, C. Serre and P. L. Llewellyn, *Eur. J. Inorg. Chem.*, 2016, **2016**, 4416–4423.
52 E. Tsalaporta and J. M. D. MacElroy, *Heliyon*, 2020, **6**, e04883.